Data Repository Item

Morphology of the Zircons

Most zircons that give Phanerozoic ages tend to be small (40-50 μm) and rounded with high-order crystal faces, consistent with grains formed during high-grade metamorphism (Vavra et al., 1999). Examples are shown in Figure DR1.

Location of the Zircons

Petrographic examination of pyroxenite and mafic granulites indicates that many samples show domains of well-equilibrated texture separated by a plexus of narrow veins, resulting either from partial melting or magma infiltration (see Song and Frey, 1989). Because of the rarity of zircons, it was not possible to identify individual crystals in thin section, but we would argue that zircons with older ages in the pyroxenites and mafic granulites are likely to be preserved in the well-equilibrated domains and that the younger zircons occur in the veins, which appear to be of several generations based on textural evidence and the zircon age data (Table DR1); thus reflecting multiple events in the lithosphere. Massive mafic granulite without veins is shown in Figure DR2a and can be compared with veined mafic granulite in Figure DR2b, the veins being of basaltic composition.

Nature of the Xenoliths

Xenoliths in the Hannuoba Basalt can be broadly divided into three categories, based on their mineralogy: (a) peridotites, which are the most voluminous and include spinel lherzolite, spinel-garnet lherzolite and websterite; (b) pyroxenites, including spinel pyroxenite and garnet pyroxenite, and (c) granulites, which are the rarest of the xenoliths, and include both two-pyroxene mafic granulite and felsic granulite.

Peridotite

The peridotite xenoliths have been described in detail in a number of papers (Song and Frey, 1989; Tatsumoto et al., 1992; Chen et al., 1998; Chen et al., 2001) and are mainly spinel lherzolite of Group I (Frey and Prinz, 1978), with rare Fe- and Ti-rich websterites of Group II. The Group 1 xenoliths consist of olivine, orthopyroxene, clinopyroxene and spinel in various proportions and are members of the Al-augite series of Wilshire and Shervais, 1975). Spinel tends to be vermicular and occurs between pyroxene crystals (Song and Frey, 1989). There is evidence of deformation in olivine and orthopyroxene and there may be some alignment of these minerals, features consistent with high temperature plastic flow (Song and Frey, 1989). The rocks show a negative correlation between MgO and CaO Al_2O_3, Na_2O and TiO_2 and they are interpreted as residues remaining after partial melting of <5% to 15-20% basalt (Song and Frey, 1989). This is also reflected in rare earth element (REE) variations, with some xenoliths enriched and some depleted in light rare earth elements (LREE). However, the pattern is not simple and there is evidence of subsequent enrichment in LREE (Song and Frey, 1989). The presence of clinopyroxene veins in such rocks is taken as evidence of a mobile mantle fluid or melt and this can result in LREE enrichment (O'Reilly and Griffin, 1988). More recently, Chen et al. (2001) have argued on the basis of similar trace element compositions for diopsides from lherzolite host and from the veins that the latter are not true veins, but the result of mechanical segregation and not metasomatism. Al-augite xenoliths are distributed throughout the lower crust and uppermost mantle: spinel-garnet lherzolite is present at depths of 55-65 km, whereas garnet pyroxenites come from >55 km depth, assuming that the southeastern Australian geotherm (SEA) of O'Reilly and Griffin (1985) is appropriate for the area. Our sample 90DA11 is from the Al-augite group and consists of clinopyroxene (60%), spinel (15%), garnet (15%), and orthopyroxene (10%).

The Group II xenoliths of Frey and Prinz (1978) are closely analogous to the Cr-diopside series of Wilshire and Shervais (1975) and consist of websterite, with some spinel pyroxenite and garnet pyroxenite. The websterites contain only ortho- and clinopyroxene. The garnet pyroxenites that are included with this group in more recent studies (Chen et al., 2001) are the olivine-poor end-members of the garnet-spinel peridotites. Our sample JSB1 is from this group and consists of clinopyroxene (50%), orthopyroxene (30%), and garnet (10%).

Pyroxenite

The pyroxenite xenoliths contain phlogopite and/or garnet and have much lower Mg/(Mg + Fe) values than the spinel-bearing peridotites (Tatsumoto et al., 1992). An exception is the pyroxenite veins (attributed to melt infiltration - Song and Frey, 1989) that cut peridotite hosts: these have similar values to the hosts. This implies Mg^{2+}-Fe^{2+} exchange equilibria between minerals in the veins and their hosts, most likely due to the high ambient temperature conditions of the lithospheric mantle below Hannuoba (Tatsumoto et al., 1992), however see Chen et al. (2001) for an alternative view. Interestingly, although there is general evidence of high temperature equilibration of major elements, the same is not true for isotopic data; there being clear evidence of isotopic disequilibria in the Nd and Sr systems (Tatsumoto et al., 1992). Extremely high $^{87}Sr/^{86}Sr$ ratios and strongly negative εNd values from a phlogopite pyroxenite - with a Nd_{DM} model age of 2.9 Ga - has been interpreted as indicating the presence of ancient metasomatised mantle lithosphere beneath Hannuoba (Tatsumoto et al., 1992). In general, the Pb isotopic compositions of the xenoliths are more radiogenic than the host Hannuoba Basalt (Tatsumoto et al., 1992), indicating the xenoliths are accidental inclusions and not cognate; they are not of cumulate origin or refractory residues after basalt extraction. Interestingly, the Pb-Pb model age for Hannuoba xenoliths is 2.65 ± 0.3 Ga - not too dissimilar to the 'background' age of the North China Craton (Zhao et al., 2001). Samples 90DA4 and 95DA16 in this study are from this group. Both consist almost entirely of pyroxene, with clinopyroxene (65%), orthopyroxene (25%) and plagioclase (10%) in 90DA4 and clinopyroxene (55%) and orthopyroxene (45%) in 95DA16.

Granulite

Two types of granulite xenoliths are represented in the Hannuoba Basalt: basic (two-pyroxene) granulites which are the most abundant, and rarer felsic granulite xenoliths. Fan et al. (1998) favored underplating of mafic magma in the late Mesozoic as the origin of the mafic granulite and this was supported by Chen et al. (2001), who suggested that the mafic granulites may be underplated basaltic magmas of Cenozoic age. Our unpublished SHRIMP ion microprobe data do not support this interpretation, since all samples of mafic granulite analyzed so far contain Archean zircons as well as Phanerozoic ones. The mafic granulites record lower equilibration temperatures (850-950°C) than the associated garnet pyroxenites and all granulites are considered to be from depths of <42 km, the depth of the Moho below the Hannuoba Basalt.

Most mafic granulite xenoliths are homogeneous, although a few are weakly layered (Chen et al., 2001). They are composed of clinopyroxene and orthopyroxene, with variable amounts of plagioclase; those with low plagioclase thus ranging to pyroxenite and websterite. The most common accessory mineral is apatite, although biotite is present in two of our samples (95-DA1/6 - see Chen et al., 2001, p.269). Samples 95DA1, 6, 7 and 17 are from this group (with some mineral chemistry for 95DA6 presented in Chen et al., 2001). The mineralogy is as follows: 95DA1 (plagioclase 90%, orthopyroxene 8%, biotite 2%); 95DA6 (plagioclase 14%, orthopyroxene 45%, clinopyroxene 45%, biotite 1%); 95DA7 (plagioclase 18%, orthopyroxene 42%, clinopyroxene 40%); 95DA17 (plagioclase 30%, orthopyroxene 30%, clinopyroxene 40%).

The felsic granulites are composed of quartz and alkali feldspar, with variable amounts of garnet and clinopyroxene. Samples 95DA37, 39 and 40 are from this group. The distribution of mafic minerals is not uniform in these rocks and so no estimates of percentages were made.

As briefly noted in the main paper, Song and Frey (1989) suggested that Rb/Sr and Sm/Nd isotopic ratios from peridotite xenoliths indicate the occurrence of depleted mantle (DM), prevalent mantle (PREMA – Zindler and Hart, 1986) and LoNd (Hart et al., 1986) types below the Hannuoba Basalt. The isotopic signature of the DM xenoliths suggests derivation from a bulk earth source at ~2 Ga ago. However, the PREMA and LoNd xenoliths reveal a more complicated evolution, suggesting several enrichment events in the depleted mantle; an ancient LREE enrichment at ~1.08 Ga ago for the LoNd xenoliths and more recent metasomatism producing the PREMA xenoliths. Such complexities were also identified by Tatsumoto et al. (1992), who favored at least two separate metasomatic events: one before 1 Ga (when the continental lithosphere gained an EM I signature) and the other at about 500 Ma or younger (when an EM II signature was introduced). As we note, this is in accord with our zircon data which indicate a whole series of events in the continental lithosphere during the Phanerozoic, but especially during the late Mesozoic (see Table DR1).

References not cited in main paper

Chen, S.H., Zhou, X.H., O'Reilly, S.Y., Griffin, W.L., Zhang, G.H., and Zhang, M., 1998. Trace element characteristics in the diopsides of peridotite xenoliths: a laser ablation-inductively coupled plasma-mass spectrometry study. Chinese Science Bulletin, v. 43, p. 579-583

Frey, F.A., and Prinz, M., 1978. Ultramafic inclusions from San Carlos, Arizona, petrologic and geochemical data bearing on their petrogenesis. Earth and Planetary Science Letters, v. 38, p. 139-176.

Zindler, A., and Hart, S.R., 1986, Chemical geodynamics: Annual Reviews of Earth and Planetary Sciences, v. 14, p. 493-571.

O'Reilly, S.Y., and Griffin, W.L., 1985. A xenolith-derived geotherm for southeastern Australia and its geographical implications. Tectonophysics, v. 111, p. 41-63.

Vavra, G., Schmidt, R., and Gebauer, D., 1999. Internal morphology, habit and U-Th-Pb microanalysis of amphibole-to-granulite facies zircons: geology of the Ivrea Zone (Southern Alps): Contributions to Mineralogy and Petrology, v. 134, p. 380-404.

Wilshire, H.G., and Shervais, J.W., 1975. Al-augite and Cr-diopside ultramafic xenoliths in basaltic rocks from western United States. Chem. Earth, v. 9, p. 257-272.

Zindler, A., and Hart, S.R., 1986, Chemical geodynamics: Annual Reviews of Earth and Planetary Sciences, v. 14, p. 493-571.

Data Repository Figure Captions

Figure DR1: Cathodoluminescence (CL) images of some of the zircon crystals analyzed in this study. A: pyroxenite zircon JSB1-8 with an age of 178 ± 7 Ma. Note weak oscillatory zoning. B: pyroxenite zircon 90DA11-3 with an age of 384 ± 4 Ma. Note elongate shape and weak oscillatory zoning. C: pyroxenite zircon 95DA16-1 with an age of 129 ± 17 Ma. Note irregular shape and lack of internal structure. D: pyroxenite zircon 95DA16-3 with an age of 123 ± 13 Ma. Note rather turbid internal structure. E: mafic granulite zircon DA1-12 with an age of 159 ± 7 Ma. Note slightly elongate shape and lack of internal structure. F: felsic granulite zircons 95DA40-8/9 with ages of 107 ± 5 Ma and 128 ± 10 Ma, respectively. Note rounded shape and weak, patchy internal zoning. White areas within crystals are traces of the SHRIMP analytical sites (ca. 15-25 μm diameter). More details on U-Pb-Th data for these grains can be obtained from Table DR1.

Figure DR2: examples of mafic xenoliths in thin section. A: massive two-pyroxene mafic granulite xenolith. B: a two-pyroxene mafic granulite xenolith traversed by thin veins and veinlets of basaltic melt. Width of images is ca. 6 mm.

TABLE DR1. U-Pb-Th ZIRCON DATA

Spot	U (ppm)	Th (ppm)	Th/U	Pb (ppm)	%comPb	$^{204}Pb/^{206}Pb$	$^{206}Pb^{*}/^{238}U$	$^{206}Pb^{*}/^{238}U$ Age
95DA16-1	17	6	0.34	0.4	15.5	0.0084	0.0201±26	129±17
95DA16-2	25	8	0.34	0.3	80.7	0.0432	0.0031±44	20±28
95DA16-3	55	51	0.97	0.9	0	0	0.0192±21	123±13
95DA16-4	30	11	0.39	0.5	37.4	0.0201	0.0113±14	73±9
95DA16-5	12	5	0.46	0.4	60.9	0.0328	0.0140±58	90±37
95DA16-6	14	7	0.47	0.3	77	0.0414	0.0053±52	34±33
90DA4-1	405	205	0.52	22.5	1.4	0.0008	0.0637±17	398±11
90DA4-2	346	51	0.15	26.2	2	0.0011	0.0863±25	534±16
90DA4-3	363	131	0.37	19.3	0.3	0.0001	0.0616±15	386±10
90DA4-4	818	257	0.32	14.8	14.4	0.0078	0.0180±5	115±3
90DA4-5	369	156	0.44	15.8	0.3	0.0001	0.0496±13	312±8
90DA4-6	215	222	1.07	9.0	3.2	0.0017	0.0470±12	296±8
90DA4-7	1032	42	0.04	56.2	0.5	0.0003	0.0631±15	394±10
90DA4-8	1516	743	0.51	29.9	2.4	0.0013	0.0224±6	143±4
90DA4-9	250	78	0.32	11.1	1.2	0.0007	0.0512±13	322±9
90DA4-10	1939	1303	0.69	42.2	4.3	0.0023	0.0243±6	154±4
90DA11-3	1248	231	0.19	68.1	3.4	0.0019	0.0613±4	384±4
JSB1-7	213	129	0.62	5.5	10.6	0.0057	0.0267±11	170±7
JSB1-8	270	257	0.99	7.2	10.1	0.0055	0.0280±11	178±7
JSB1-1	206	202	1.01	5.5	22.8	0.0124	0.0239±15	153±10
JSB1-3	397	244	0.64	10.1	6.9	0.0038	0.0276±12	175±8
JSB1-4	816	445	0.56	29.7	2.6	0.0014	0.0413±13	261±8
JSB1-5	76	60	0.82	2.6	38.3	0.0208	0.0247±22	157±14
95DA1-1	6	1	0.13	0.1	0	0	0.0236±13	151±8
95DA1-2	6	1	0.14	0.1	0	0	0.0226±17	144±11
95DA1-3	8	1	0.13	0.1	0	0	0.0245±12	156±7
95DA1-4	7	1	0.13	0.1	56.2	0.0302	0.0097±49	62±32
95DA1-5	5	3	0.56	0.1	0	0	0.0343±45	217±28
95DA1-7	6	1	0.10	0.1	62.8	0.0338	0.0097±63	62±40
95DA1-9	5	1	0.11	0.1	28.3	0.0153	0.0188±039	120±25
95DA1-10	6	1	0.11	0.1	46.8	0.0252	0.0130±40	83±26
95DA1-11	7	1	0.12	0.1	36.5	0.0197	0.0133±43	85±27
95DA1-12	6	0	0.07	0.1	0	0	0.0250±12	159±7
95DA1-13	4	0	0.10	0.1	20.2	0.0109	0.0194±121	124±77
95DA1-15	57	11	0.20	3.4	1.1	0.0006	0.0681±127	424±77
95DA1-17	841	85	0.10	22.5	0	0	0.0312±32	198±20
95DA6-2	297	322	1.12	5.2	1.4	0.0007	0.0200±11	128±7
95DA6-3	25	11	0.46	0.4	23.7	0.0128	0.0149±10	95±6
95DA6-5	92	46	0.52	1.0	7.8	0.0042	0.0118±7	75±5
95DA6-6	412	269	0.68	26.8	0.4	0.0002	0.0752±39	468±24
95DA6-7	29	13	0.48	0.5	17.7	0.0095	0.0166±15	106±10

Spot	U (ppm)	Th (ppm)	Th/U	Pb (ppm)	%comPb	$^{204}Pb/^{206}Pb$	$^{206}Pb^{*}/^{238}U$	$^{206}Pb^{*}/^{238}U$ Age
95DA7-4	108	62	0.60	5.7	7.8	0.0043	0.0564±32	354±20
95DA7-6	10	5	0.52	0.2	15.9	0.0086	0.0235±35	150±22
95DA7-7	120	68	0.59	3.6	2	0.0011	0.0343±50	218±31
95DA17-6	411	254	0.64	25.4	0.3	0.0002	0.0718±4	447±5
95DA17-10	199	41	0.21	10.8	1.5	0.0008	0.0626±6	391±5
95DA37-1	143	53	0.38	1.6	0	0	0.0134±4	86±2
95DA37-2	50	52	1.08	0.9	5.8	0.0031	0.0194±11	124±7
95DA37-3	35	15	0.46	0.8	2.9	0.0016	0.0257±13	164±8
95DA37-4	26	11	0.44	0.5	8.9	0.0048	0.0197±22	126±14
95DA37-5	63	29	0.47	1.5	3.5	0.0019	0.0265±9	168±6
95DA37-6	21	10	0.50	0.4	7	0.0038	0.0190±37	121±24
95DA37-7	76	34	0.46	1.7	0	0	0.0262±11	167±7
95DA37-8	86	112	1.36	1.7	6	0.0032	0.0223±12	142±8
95DA37-9	8	4	0.55	0.2	41.1	0.0222	0.0147±25	94±16
95DA37-10	117	96	0.85	3.6	2.3	0.0012	0.0349±43	221±27
95DA37-11	24	12	0.49	0.4	0	0	0.0196±10	125±6
95DA37-12	19	9	0.50	0.3	6.4	0.0034	0.0184±10	117±6
95DA37-13	20	9	0.49	0.3	17.6	0.0095	0.0162±10	103±6
95DA40-1	12	6	0.50	0.3	20.6	0.0111	0.0219±20	140±13
95DA40-2	11	4	0.40	0.3	32	0.0173	0.0193±33	123±21
95DA40-3	15	6	0.43	0.8	11.8	0.0065	0.0519±53	326±33
95DA40-4	13	6	0.45	0.3	15.3	0.0083	0.0194±18	124±11
95DA40-5	95	90	0.99	1.5	6	0.0033	0.0178±6	114±4
95DA40-6	20	8	0.43	0.3	32.5	0.0175	0.0135±17	86±11
95DA40-7	57	33	0.60	0.8	7.4	0.004	0.0148±13	94±8
95DA40-8	68	48	0.73	1.1	12.1	0.0065	0.0167±8	107±5
95DA40-9	11	5	0.47	0.2	12.6	0.0068	0.0200±16	128±10
95DA40-10	12	5	0.43	0.2	0	0	0.0248±12	158±8
95DA40-11	283	104	0.38	4.3	4.9	0.0026	0.0168±7	107±4
95DA40-12	31	22	0.74	0.4	24.7	0.0133	0.0124±20	80±13
95DA39-1	467	380	0.84	12.1	0.1	0.0001	0.0302±10	192±7
95DA39-2	7	3	0.43	0.1	28.8	0.0155	0.0147±30	94±19
95DA39-3	91	104	1.18	1.2	3.8	0.002	0.0142±7	91±5
95DA39-4	144	149	1.07	5.8	0.7	0.0004	0.0466±31	293±19
95DA39-5	26	11	0.46	0.4	4.9	0.0026	0.0167±9	107±6
95DA39-6	43	21	0.50	0.6	0	0	0.0153±5	98±3
95DA39-7	83	99	1.23	1.9	0	0	0.0274±7	174±5
95DA39-8	159	117	0.76	2.8	1.2	0.0006	0.0203±8	130±5
95DA39-9	103	45	0.45	1.4	2	0.0011	0.0159±5	102±3
95DA39-10	6	3	0.43	0.1	31.7	0.0171	0.0152±39	97±25
95DA39-11	96	58	0.63	1.3	2	0.0011	0.0158±5	101±3
95DA39-12	5	2	0.39	0.1	23.2	0.0125	0.0178±31	114±19
95DA39-13	24	11	0.48	0.4	5.8	0.0031	0.0195±12	124±8

Wilde, S.A. Fig. DR1

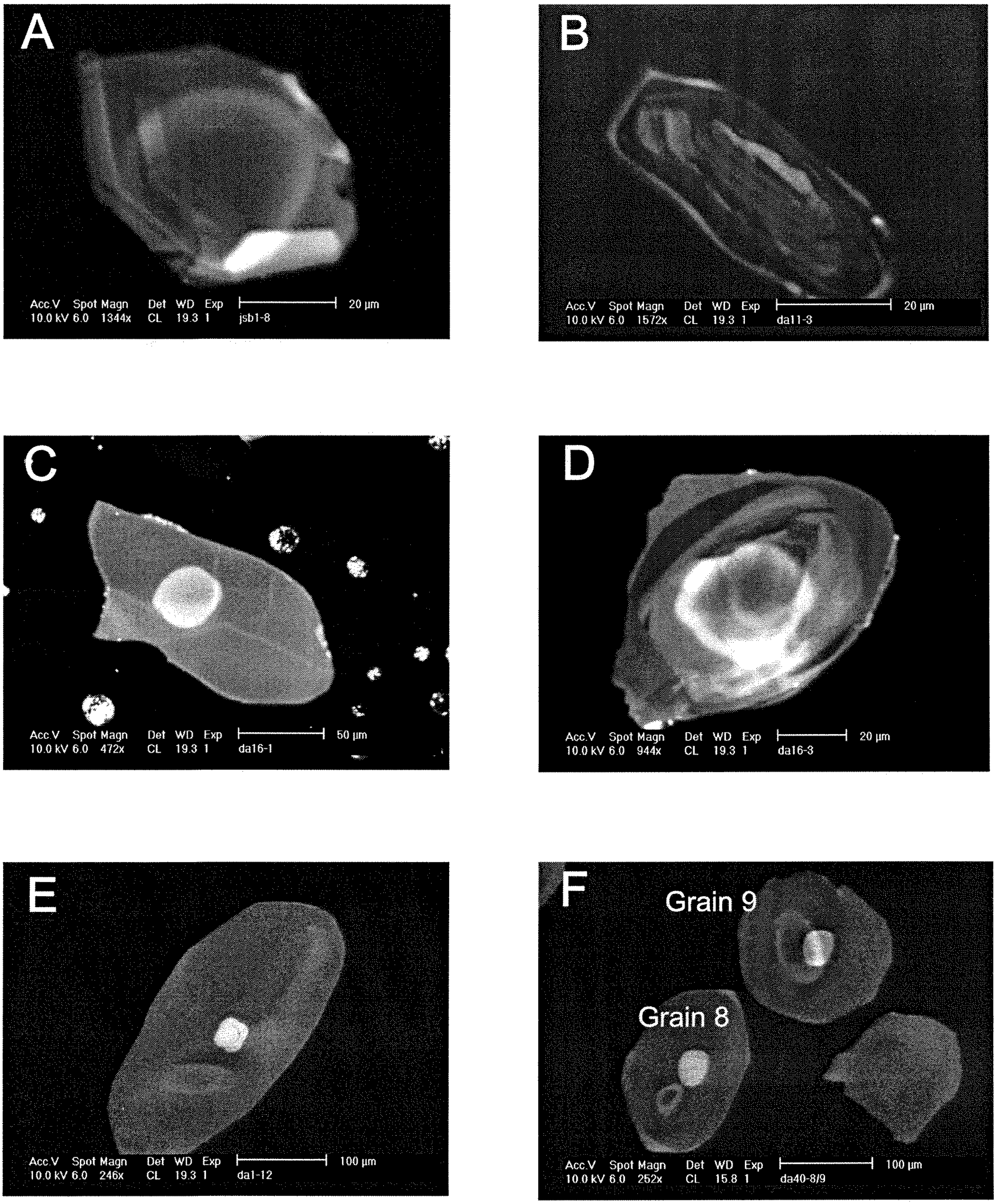

Wilde, S.A. Fig. DR2